universe

MDPI

Article

Probing Dense Nuclear Matter in the Laboratory: Experiments at FAIR and NICA

Peter Senger [1,2]

[1] Facility for Antiproton and Ion Research, 64291 Darmstadt, Germany; p.senger@gsi.de
[2] MEPhI (Moscow Engineering Physics Institute), National Research Nuclear University, 115409 Moscow, Russia

Abstract: The poorly known properties of high-density strongly-interacting matter govern the structure of neutron stars and the dynamics of neutron star mergers. New insight has been and will be gained by astronomical observations, such as the measurement of mass and radius of neutron stars, and the detection of gravitational waves emitted from neutron star mergers. Alternatively, information on the Nuclear Matter Equation-of-State (EOS) and on a possible phase transition from hadronic to quark matter at high baryon densities can be obtained from laboratory experiments investigating heavy-ion collisions. Detector systems dedicated to such experiments are under construction at the "Facility for Antiproton and Ion Research" (FAIR) in Darmstadt, Germany, and at the "Nuclotron-based Ion Collider fAcility" (NICA) in Dubna, Russia. In heavy-ion collisions at these accelerator centers, one expects the creation of baryon densities of up to 10 times saturation density, where quark degrees-of-freedom should emerge. This article reviews the most promising observables in heavy-ion collisions, which are used to probe the high-density EOS and possible phase transition from hadronic to quark matter. Finally, the facilities and the experimental setups will be briefly described.

Keywords: heavy-ion collisions; nuclear equation-of-state; QCD phase diagram

Citation: Senger, P. Probing Dense Nuclear Matter in the Laboratory: Experiments at FAIR and NICA. *Universe* **2021**, 7, 171. https://doi.org/10.3390/universe7060171

Academic Editors: Rosa Poggiani and Ignazio Bombaci

Received: 8 May 2021
Accepted: 28 May 2021
Published: 30 May 2021

1. Introduction

An intriguing aspect of heavy-ion experiments is the prospect to investigate important features of cosmic matter in the laboratory. In a central heavy-ion collision at a beam energy of 5 GeV/nucleon, for example, the nucleons pile up in the transient fireball to densities of more than 5 times saturation density ρ_0, a condition which is also expected to prevail in the core of a neutron star. Both in neutron stars and heavy-ion collisions, the maximum density is limited by the Equation-of-State (EOS) of nuclear matter. Once the EOS is known, one can calculate the mass and radius of neutron stars by the Tolman-Oppenheimer-Volkoff (TOV) equation. This is illustrated in Figure 1, which depicts masses and central densities of neutron stars calculated using different EOS [1]. Some of the EOS are ruled out by the most massive neutron stars indicated in Figure 1, such as the millisecond pulsar PSR J0740 + 6620 with a mass of 2.08 ± 0.07 solar masses [2], and PSR J1614 − 2230 with a mass of 1.908 ± 0.016 solar masses [3]. According to the EOS shown in Figure 1, densities of about 4 ρ_0 are reached in massive stars.

The EOS of dense nuclear matter has been and still is studied both via astronomical observations and in heavy-ion collision experiments. The Neutron Star Interior Composition Explorer (NICER) satellite, which is located at the International Space Station since 2017, measures the energy and time of X-rays emitted from the hot spots of millisecond pulsars, in order to extract from these data information on the mass and radius of the neutron star [4]. For example, NICER has determined a radius of $R = 13.7 + 2.6 - 1.5$ km for the most massive pulsar PSR J0740 + 6620 indicated in Figure 1. From these measurements, constraints of the EOS have been inferred, as will be discussed below.

In the case of heavy-ion collisions, the pressure inside the reaction volume drives the collective motion of the particles, and the strength of the resulting flow represents a barometer. Moreover, the number of strange particles produced by multiple collisions at subthreshold beam energies increases with the increasing density in the reaction volume. Consequently, both the collective flow of particles and the yield of particles produced at subthreshold beam energies serve as diagnostic probes of the EOS. The EOS of neutron rich matter can be investigated in heavy-ion collision by the measurement of the collective neutron flow, and of the yield of particles with opposite isospin. An open issue is the role of hyperons in neutron stars, which can also be addressed in heavy-ion collisions by measuring the lifetime and mass of the produced hypernuclei, which provide information on the ΛN, ΛNN, and ΛΛN interactions.

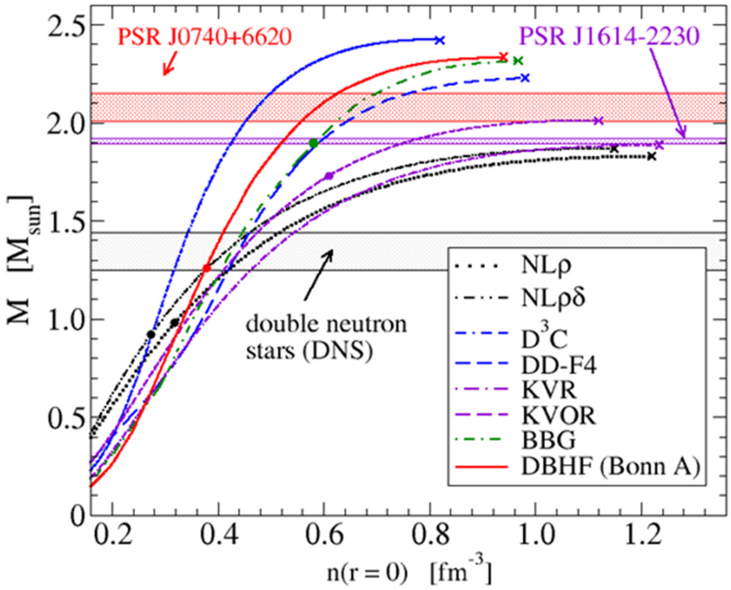

Figure 1. Neutron star mass versus central density for different EOS [1].

At baryon densities beyond 4–5 ρ_0, it is expected that nucleons start to dissolve, and quark degrees-of-freedom emerge [5]. Such a quark-hadron phase transition might be continuous, as predicted for very high temperatures prevailing in the early universe or in the fireball created in heavy-ion collisions at ultra-relativistic energies. At lower temperatures and higher densities, i.e., under conditions, which exist in the fireball created during heavy-ion collisions at intermediate beam energies, in the core of neutron stars, and in the collision zone of neutron star mergers, the transition might be of first order, featuring phase coexistence and a critical endpoint. Experimentally, such a transition is expected to leave its traces in certain observables of heavy-ion collisions, and in the frequency spectra of gravitational waves emitted in a neutron star merger. In conclusion, despite their tiny size, short lifetime and dynamic evolution, heavy-ion collisions offer the opportunity to investigate properties of dense, strongly interacting matter, which are relevant for our understanding of compact stellar objects. In this article, promising laboratory experiments on the exploration of dense baryonic matter will be discussed, which are part of the physics programs of the future accelerator facilities FAIR and NICA.

2. The High-Density Equation-of-State of Nuclear Matter

In the laboratory, information on the EOS has been extracted from the collective flow of particles generated in a collision between heavy nuclei, and from the yield of strange particles measured in heavy-ion collisions at subthreshold bombarding energies, as it will be discussed in the following sections.

The EOS relates pressure, density, volume, temperature, and isospin. For a constant temperature, the pressure can be written as $P = \rho^2\, d(E/A)/d\rho$ with ρ the density and the binding energy per nucleon $E/A(\rho,\delta) = E/A(\rho,0) + E_{sym}(\rho)\cdot\delta^2 + O(\delta^4)$, where E_{sym} is the symmetry energy and $\delta = (\rho_n - \rho_p)/\rho$ the isospin asymmetry parameter. A characteristic parameter of the EOS is the nuclear incompressibility $K_{nm} = 9\rho^2\, d^2(E/A)/d\rho^2$, which describes the curvature of E/A at saturation density ρ_0, where E/A has its minimum at −16 MeV. At saturation density, values of $250\ \text{MeV} < K_{nm}(\rho_0) = 315$ MeV have been determined by the analysis of measured giant monopole resonances in heavy nuclei [6]. Various examples of the EOS for symmetric matter and for neutron matter are shown in Figure 2 [7].

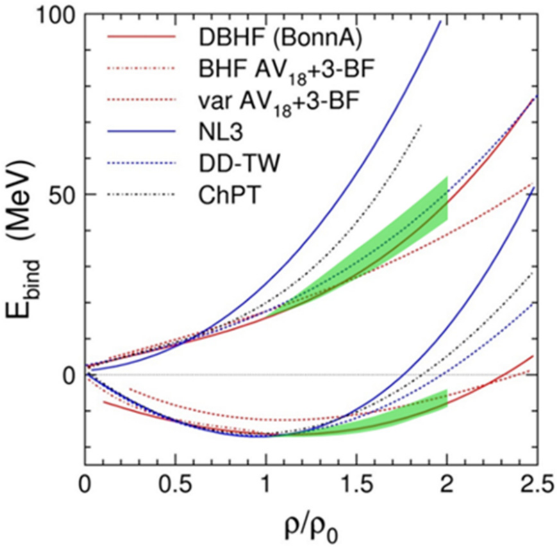

Figure 2. Various equations-of-state for isospin-symmetric nuclear matter (lower curves) and neutron matter (upper curves) as a function of baryon density. Taken from [7]. The green areas are consistent with data taken at GSI [8–13], see text.

In order to obtain the EOS relevant for neutron stars, both $E/A(\rho,0)$ and $E_{sym}(\rho)$ have to be measured at higher densities. In heavy-ion collisions, an important diagnostic probe for the EOS is the collective flow of particles, which is driven by the pressure gradient in the compressed reaction volume. For example, the collective flow of charged particles is sensitive to the EOS for symmetric matter, whereas the flow of neutrons carries information on the symmetry energy.

Densities above 2 ρ_0 can be created in Au + Au collisions at beam kinetic energies up to 1.5A GeV, as illustrated in Figure 2. The FOPI collaboration performed a systematic investigation of the elliptic flow of protons and light fragments in Au + Au collisions at energies from 0.4 to 1.5A GeV. A comparison of the data to the results of a simulation with an IQMD event generator, which takes into account momentum dependent interactions and in-medium cross sections, extracted a value of $K_{nm} = 190 \pm 30$ MeV for the incompressibility [8]. A more recent comparison of the data to results of UrQMD transport calculations, which take into account a Skyrme potential energy-density functional, found a value of $K_{nm} = 220 \pm 40$ MeV [9]. Both results confirm a soft EOS for densities between 1 and 2 ρ_0. The KaoS collaboration at GSI developed a complementary method to explore the EOS for symmetric matter, which is the measurement of K^+ mesons in Au + Au collisions at beam energies from 0.8 to 1.5A GeV [10]. At these beam energies, which are below the threshold energy of 1.6 GeV for nucleon-nucleon collisions, K^+ mesons are produced in sequential collisions of nucleons, resonances, and pions. The amount of these multiple-step collisions, and, hence, the number of produced K^+ mesons, increase with the increasing density, i.e., with the softness of the EOS. It turned out, that it is important to also measure a reference system such as C + C, where K^+ yield is not sensitive to the EOS, but to effects such as the nucleon momentum distribution and short-range correlations. The ratio of K^+ mesons measured in Au + Au over C + C collisions could be reproduced by transport model calculations assuming a nuclear incompressibility of $K_{nm} \approx 200$ MeV [11,12] for densities up to about 2 ρ_0. The resulting EOS for symmetric matter measured by the FOPI and KaoS experiments is shown as the lower green area in Figure 2.

In order to determine the EOS for neutron matter, the symmetry energy E_{sym} has to be measured in addition to the EOS for symmetric matter. One of the experimental observables in heavy-ion collisions sensitive to E_{sym} is the elliptic flow of neutrons. Such a measurement has been performed at GSI by the ASY-EOS collaboration, which determined the elliptic flow of neutrons and of protons in Au + Au collisions at a beam energy of 0.4A GeV [13]. The data could be reproduced by a UrQMD transport calculation, which extracted the E_{sym} up to densities up to 2 ρ_0, where the symmetry energy reaches a value of $E_{sym} = 55 \pm 5$ MeV. When adding the density dependent symmetry energy measured by the Asy-EOS collaboration to the EOS for symmetric matter measured by FOPI and KaoS, one obtains the EOS relevant for neutron stars up to densities of about 2 ρ_0. The result is shown in Figure 2 as the upper green area. It is worthwhile to note that the relativistic Dirac-Brueckner-Hartree-Fock (DBHF) approach provides a soft EOS up to densities of about $2\rho_0$ in agreement with the experiments, which then stiffens towards higher densities as required for the most massive neutron stars (see Figure 1).

The pion multiplicity ratio π^-/π^+ is also expected to be sensitive to the symmetry energy E_{sym} at high densities, as pions are produced via decays of delta resonances, which reflect the density of protons and neutrons. However, the interpretation of the π^-/π^+ multiplicity ratio measured so far in collisions between stable nuclei has not provided a consistent picture [14]. In contrast, the ratios of the charged pion spectra at high transverse momenta, measured in collisions of rare Sn isotopes with different isospins, provided constrains of the symmetry energy, which are comparable to the results obtained from the flow ratio of neutrons and protons [15].

From the EOS for neutron matter, as illustrated by the upper green area in Figure 2, one can estimate the pressure, which is in the range from about 20 to 40 MeV/fm^3 for a density of 2 ρ_0. The pressure of neutron star matter as a function of density has been also derived from combined results of NICER measurements of several pulsars, including PSR J0740 + 6620, and the tidal deformability estimate from the GW170817 event [16]. In this case, the extracted pressure values vary between about 15 MeV/fm^3 and about 60 MeV/fm^3 at a density of 2 ρ_0. This comparison illustrates, that laboratory experiments and astronomical observations can be used as complementary methods to determine the EOS for neutron stars.

In order to extend EOS measurements in the laboratory towards higher densities, the beam energy has to be increased. Densities of up to 5 ρ_0, which are expected to prevail in the core of neutron stars, have been produced in heavy-ion collisions at the AGS in Brookhaven. These experiments measured both the transverse and elliptic flow of protons in Au + Au collisions at energies between 2 and 11A GeV [17]. The data have been compared to results of relativistic transport model calculations, which could reproduce the transverse (direct) flow data under the assumption of a soft EOS ($K_{nm} = 210$ MeV), and the elliptic flow data assuming stiff EOS ($K_{nm} = 300$ MeV) [18]. A compilation of the results of the heavy-ion experiments with respect to the EOS for dense symmetric nuclear matter is shown in Figure 3, which depicts the pressure as a function of baryon density. The grey-hatched area is consistent with the AGS data, while the yellow area indicates the results of the GSI experiments [8–13]. The blue and red lines represent transport model calculations for a soft and a hard EOS, respectively [18].

As illustrated in Figure 3, the constraint on the EOS for symmetric matter at higher densities, represented by the grey hatched area, is not very conclusive, as it only excludes very soft or very hard EOS. The reason is that the interpretation of the direct flow and the elliptic flow yielded different values for the nuclear incompressibility. The upcoming experiments at FAIR and NICA will perform precision measurements of the collective flow of protons and light fragments in heavy-ion collisions, in order to reduce the uncertainties of the EOS indicated in Figure 3. Moreover, extrapolating the concept of subthreshold particle production to higher energies, detailed measurements of multi-strange (anti-) hyperons will be performed for the first time at beam energies between 2 and 11A GeV, in order to study the high-density EOS of symmetric matter at neutron star core densities. This approach is supported by calculations with the new PHQMD event generator, which predicts for Au + Au collisions at an energy of 4A GeV a factor of 2 higher $\Xi^{\pm}$ and $\Omega^{\pm}$ hyperon yields for a soft compared to a hard EOS [19].

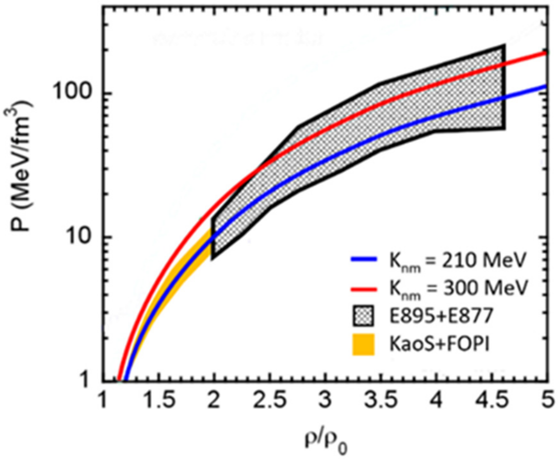

Figure 3. Pressure as a function of baryon density for symmetric nuclear matter. The grey hatched area represents the constraint provided by proton flow data taken at AGS [17,18]. Yellow area: Constraint from fragment flow and kaon data taken at GSI [8–13]. Red line: Hard EOS, blue line: Soft EOS [18].

In order to contribute to our understanding of neutron stars, future experiments should also extend the measurement of the symmetry energy towards higher beam energies and densities. In addition to the collective flow of neutrons, also particles with opposite isospin I_3 are considered to be sensitive to E_{sym}. Promising observables reflecting the density of neutrons (ddu) and protons (uud) are Σ^-(dds) and Σ^+(uus) hyperons, which differ in isospin by $I_3 = \pm 1$. However, the identification of these hyperons in heavy-ion collisions is experimentally challenging, since one of their decay daughters is neutral. Easier to measure are excited Σ^{*-}(dds) and Σ^{*+}(uus) hyperons which decay into $\Lambda\pi$ pairs. In both cases, the identification of the hyperons requires the precise measurement of the decay vertex by a high-resolution tracking device.

3. Hyperons in Dense Matter

The EOS of dense matter in beta-equilibrium will be substantially softened, if the chemical potential of neutrons exceeds the chemical potential of hyperons. This effect would prohibit the formation of massive neutron stars such as PSR J0740 6620. Various solutions for this "hyperon puzzle" have been proposed, in order to prevent the condensation of hyperons in neutron stars. A decisive role in this respect plays the ΛN interaction, and in particular, three-body forces such as the ΛNN interaction [20,21], which become increasingly important at high densities. An example is shown in Figure 4, which presents the results of a calculation based on the chiral effective field theory extended with Functional Renormalization Group (FRG) methods [21]. The chemical potential of the lambda has been calculated with ΛN interactions only (blue dashed curve), and with ΛN and ΛNN interactions (blue solid curve). In the first case, the decay of neutrons into lambdas, and, hence, the softening of the EOS, already happens at moderate densities of about 3.5 ρ_0. Taking into account the NNΛ interactions, this effect happens at much higher energies, and allows the formation of massive neutron stars.

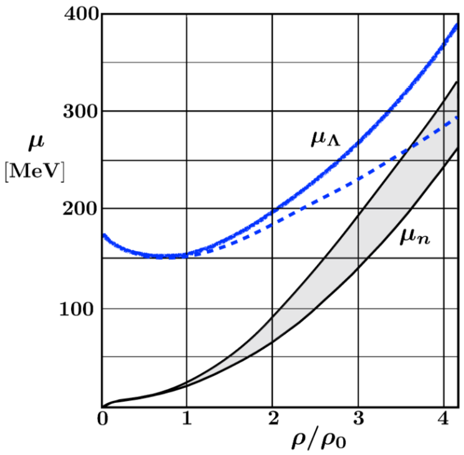

Figure 4. Chemical potentials of Λ hyperon μ_Λ and neutron μ_n in neutron matter versus baryon density (in units of saturation density). The neutron chemical potential (grey shaded area) is based on a chiral FRG calculation. The blue dashed line indicates the Λ chemical potential calculated with ΛN interactions only, whereas the blue solid line refers to a calculation taking into account both ΛN and ΛNN interactions [21].

A promising option to study experimentally the ΛN, ΛNN, and even the ΛΛN interaction, is to measure precisely the lifetime and binding energies of (double-) lambda hypernuclei. According to statistical model calculations, heavy-ion collisions at FAIR and NICA energies are a rich source of hypernuclei [22]. This is caused by the fact, that the yield of light nuclei increases with the decreasing collision energy, while the yield of lambdas increases with the increasing collision energy, and the resulting maximum of the hypernuclei yield is found at collision energies around $\sqrt{s_{NN}}$ = 4 GeV. At this energy, the production probability per central Au + Au collision is 2×10^{-2} for ${}^{3}{}_{\Lambda}$H nuclei, about 5×10^{-6} for ${}^{5}{}_{\Lambda\Lambda}$H nuclei, and about 1×10^{-7} for ${}^{5}{}_{\Lambda\Lambda}$He nuclei. Assuming a collision rate of 1 MHz, as it is planned for the CBM experiment at FAIR, and a reconstruction efficiency of 1%, one can expect to measure about 100 ${}^{3}{}_{\Lambda}$H nuclei per second, about 180 ${}^{5}{}_{\Lambda\Lambda}$H nuclei per hour, and about 80 ${}^{5}{}_{\Lambda\Lambda}$He nuclei per day. These numbers will be slightly reduced by the branching ratio of the decay $\Lambda \rightarrow p\pi^-$, which is 0.64 for the free lambda. Under such conditions, also the discovery of yet unknown hypernuclei is highly probable.

4. Searching for Quark Degrees-of-Freedom at High Baryon Densities

Already a few microseconds after the big bang a QCD phase transition happens: The primordial soup of quarks and gluons expands, cools down, and finally condenses into hadrons. A similar quark-hadron phase transition can be studied in the laboratory in heavy-ion collisions at ultra-relativistic energies as available at CERN-LHC and BNL-RHIC. Such collisions produce an extremely hot fireball consisting of quark-gluon matter, which also expands, cools down, and finally hadronizes. The yields of all produced particles can be reproduced with a Statistical Hadronization Model assuming a freeze-out temperature of $T_{fo} = 156.5 \pm 1.5$ MeV at zero baryon chemical potential μ_B [23]. This freeze-out temperature coincides with the pseudo-critical temperature of $T_c = 154 \pm 9$ MeV, which is predicted for a smooth crossover transition from quark-gluon to hadronic matter for $\mu_B = 0$ by the fundamental theory of strong interaction, Quantum Chromo Dynamics (QCD) [24,25]. Recent lattice QCD calculations found an upper limit of the critical temperature of a chiral phase transition for massless quarks at $\mu_B = 0$ of ${T_c}^0 = 132 + 3 - 6$ MeV [26].

The degrees-of-freedom of QCD matter at high baryon densities are much less understood. Due to the sign problem, lattice QCD calculations cannot be performed reliably for finite baryon chemical potentials. However, it is very likely that nucleons start to penetrate each other at densities above 4–5 ρ_0, and various models predict a transition from hadronic to quark matter [27], which might be continuous or of first order. An example for a 1st order transition occurring in a neutron star merger event is illustrated in Figure 5 [28].

The left panel of Figure 5 illustrates the rest-mass density in the equatorial plane of a merger of two neutron stars each with 1.35 solar masses, simulated assuming an EOS with a 1st order phase transition. The black dashed circle indicates the onset of deconfinement, while the blue circle contains the region of pure quark matter. The right panel of Figure 5 depicts the corresponding rest-mass distribution of the matter as a function of density and temperature. The black dashed line indicates the onset of deconfinement, which happens for low temperatures at densities of about 3 ρ_0. The black solid line represents the boundary for pure quark matter, which prevails at densities above 4 ρ_0.

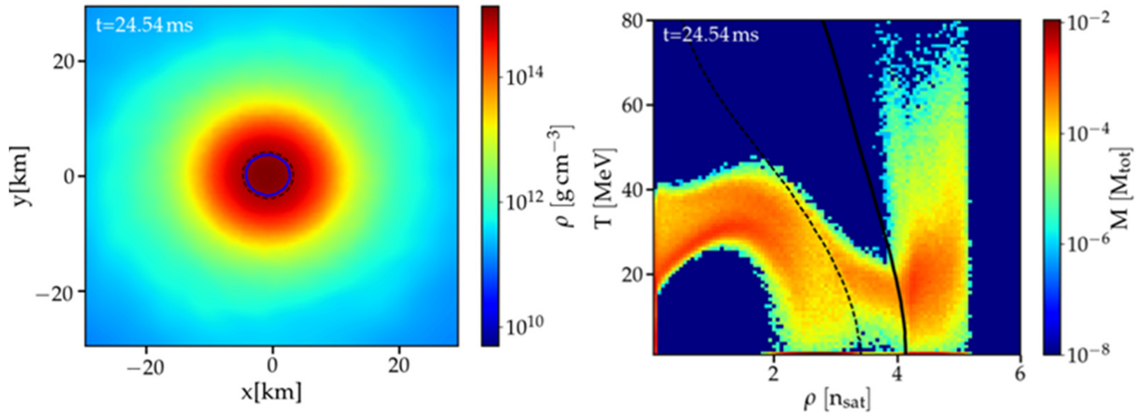

Figure 5. Simulation of a merger of two neutron stars each with 1.35 solar masses based on an EOS with a 1st order phase transition. Left: Rest mass density in the equatorial plane. The black dashed line and the solid blue line surround the regions of phase coexistence and quark matter, respectively. Right: Rest mass distribution as a function of density and temperature plane normalized to the total mass of the system. The black dashed line illustrates the onset of the hadron-quark phase transition. The solid black line is the boundary of the pure quark matter phase. Taken from [28].

One experimental possibility to prove the existence of a 1st order phase transition in neutron stars as illustrated in Figure 5, is to detect an increase of the post-merger gravitational wave frequency relative to the premerger phase [28]. In the laboratory, baryon densities of 5 ρ_0 and above can be reached in heavy-ion collisions at FAIR and NICA beam energies, which opens the possibility to explore the degrees-of-freedom of high-density isospin-symmetric QCD matter. Moreover, according to the recent lattice QCD calculation mentioned above, which found an upper limit of the chiral critical point for $\mu_B = 0$ at $T_c^0 \approx 130$ MeV, the critical endpoint for non-zero quark masses at finite μ_B is located at even lower temperatures, if it exists at all. Again, such temperatures can be easily reached in heavy-ion collisions at beam energies available at FAIR and NICA. Possible experimental observables, which are expected to be sensitive to a hadron-quark phase transition at high densities and intermediate temperatures, will be discussed in the following sections.

4.1. Fluctuations of Net-Proton Number Distributions

The STAR collaboration at RHIC executes a heavy-ion beam energy scan program in order to systematically study the features of the QCD phase diagram. An important aspect of this program is the search for the critical endpoint of a 1st order phase transition, which is expected to be located at large baryon chemical potentials. The fluctuation of higher moments of the baryon number distribution has been suggested as a promising signature of the critical endpoint [29], in analogy to the effect of critical opalescence in classical binary systems. As a proxy for the baryons, the STAR collaboration measured the net-protons, and studied in detail the shape of their multiplicity distribution event-by-event, in order to determine the higher order cumulants [30]. Figure 6 depicts the resulting ratios of the 3rd to the 2nd cumulant C_3/C_2 (=$S\sigma$) (left panel) and the 4th to the 2nd cumulant C_4/C_2 (=$\kappa\sigma^2$) (right panel) as a function of beam energy for central and peripheral Au + Au collisions. The data are compared to results of the Hadron Resonance Gas (HRG) model and the UrQMD event generator. For the lowest collision energy of $\sqrt{s_{NN}} = 7.7$ GeV, a non-monotonic variation in kurtosis × variance $\kappa\sigma^2$ was determined with a significance of 3.1σ. Further investigations, in particular at lower energies, are required to clarify the situation. Such experiments will be performed at STAR with a fixed target, at NICA with the BM@N and MPD experiments, and at FAIR with the CBM setup. It is worthwhile to note, that the FAIR-NICA beam energy range is particularly interesting in view of the result of recent lattice QCD calculations mentioned above, which restrict the location of a possible critical endpoint to temperatures below about 130 MeV, i.e., to collision energies below about $\sqrt{s_{NN}}$ = 6 GeV.

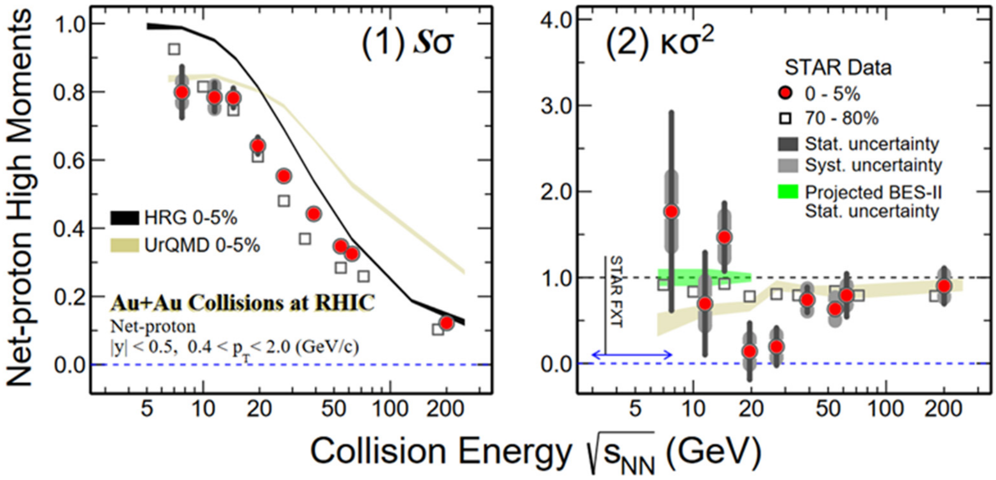

Figure 6. $S\sigma$ (1) and $\kappa\sigma^2$ (2) as a function of collision energy for net-proton distributions measured in Au + Au collisions (see text). Taken from [30].

4.2. Chemical Equilibration of Multi-Strange (Anti-) Hyperons

Statistical models are very successful in describing the yields of particles produced in high-energy heavy-ion collisions by fitting three parameters assuming chemical equilibrium: Temperature, baryon-chemical potential, and volume [31–33]. The resulting freeze-out temperature characterizes the situation, where the particles cease to interact inelastically. Even the yield of light (anti-) nuclei and hypernuclei can be reproduced for heavy-ion collisions at LHC energies, where the particles freeze out at a temperature of T_{fo} = 156.5 ± 1.5 MeV, although the binding energies of the light nuclei are in the order of MeV [23]. Moreover, (multi-) strange (anti-) hyperons freeze out at this temperature. Due to the small hyperon-nucleon scattering cross section, it is very unlikely that they chemically equilibrate in the short lifetime of the dense hadronic phase. Moreover, as mentioned above, the freeze-out temperature coincides with the pseudo-critical temperature of the crossover phase transition obtained from the lattice QCD calculation. Therefore, the hyperons are expected to be driven into chemical equilibrium by the hadronization process during the phase transition [34]. Consequently, the observation of chemically equilibrated multi-strange hyperons can serve as a signature for a phase transition. Moreover, in heavy-ion collisions at a beam energy of 30A GeV, the yield of Ξ and Ω hyperons is in agreement with the assumption of chemical equilibrium [35]. The heavy-ion collision system with the lowest beam energy, where double-strange Ξ^- hyperons have been observed so far, was Ar + KCl at 1.76A GeV. In this case, the Ξ^- yield is a factor of 24 ± 9 above the prediction of the statistical model, which, however, is able to explain the yield of all other particles with a chemical freeze-out temperature of 70 ± 3 MeV and a baryon chemical potential of μ_B = 748 ± 8 MeV [36]. Future experiments at FAIR and NICA will measure the yields of $\Xi^{\pm}$ and $\Omega^{\pm}$ hyperons in Au + Au collisions from beam energies of 2 to 30A GeV ($\sqrt{s_{NN}}$ = 7.7 GeV) and higher, in order to identify the temperature and the baryon-chemical potential, where multi-strange (anti-) hyperons reach chemical equilibration, which might coincide with the onset of deconfinement.

4.3. Charmonium as a Probe of Deconfinement

The observed large charmonium yield in central heavy-ion collisions at LHC is interpreted as one of the most convincing signatures for the creation of the Quark-Gluon-Plasma [37]. The Statistical Hadronization Model (SHM) is able to reproduce the data, by assuming initial hard collisions producing the charm and anticharm quarks, which then thermalize in the Quark-Gluon-Plasma, and finally statistically hadronize at the phase boundary into J/ψ mesons, D mesons, and Λ_c hyperons [37]. In hadronic scenarios such as the Hadron-String-Dynamics (HSD) transport code, hadrons with charm quarks are created, for example, in processes such as pp → J/ψ pp, pp → anti-D Λ_c p, and pp → D anti-D pp [38]. These hadronic reactions have different threshold energies, in contrast to the statistical hadronization picture. Consequently, the two models predict different yields of particles with charm quarks, in particular for beam energies close to the production thresholds. The difference for central Au + Au reactions is illustrated in Figure 7, which depicts the (J/ψ)/(D+anti-D) ratio versus collision energy. The red (blue) symbols represent the results of the HSD (SHM) calculations. In the hadronic scenario, this ratio increases strongly with decreasing collision energies, due to the lower J/ψ threshold, whereas for the SHM the ratio is nearly constant. Presently, no charm data exist for heavy-ion collisions in the FAIR and NICA energy range. Future experiments at these facilities will investigate charm production mechanisms close to threshold beam energies, in order to explore the degrees-of-freedom of QCD matter at high densities.

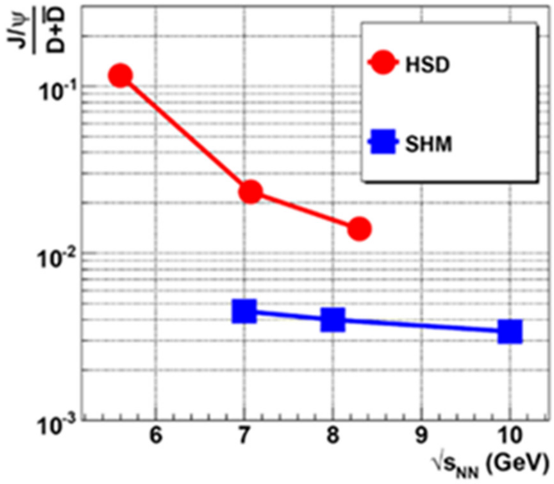

Figure 7. The (J/ψ)/(D+anti-D) ratio simulated for central Au+Au collisions at different collision energies with SHM (blue symbols) [37] and with the HSD code (red symbols) [38].

Within the UrQMD transport code, charm production mechanisms in heavy ion collisions below the production energy have been proposed [39]. The model predicts multiple hadron-hadron collisions resulting in the excitation of heavy N* resonances, which finally decay via N* → J/ψ + N + N and N* → Λ_c + anti-D into charmed particles. The observation of charm particles below threshold energies would shed a new light on the charm production mechanisms in heavy-ion collisions, and would open the possibility to use charm as a probe of dense baryonic matter.

4.4. Dilepton Radiation from the Hot and Dense Fireball

Dileptons radiated away from the fireball in heavy-ion collisions reflect the extreme conditions, which prevail inside the hot and dense reaction volume. For example, the dilepton invariant mass spectrum contains information on the in-medium properties of vector mesons, which decay into lepton pairs. As leptons do not suffer from re-scattering, the information on the spectral shape is not disturbed by the final-state interaction. Moreover, lepton pairs offer the unique opportunity to measure the average temperature of the fireball. This information can be directly extracted from the shape of the invariant mass spectrum, in particular from the mass range above the ϕ meson (1 GeV/c^2), which contains only very little contributions from the decay of vector mesons. It is worthwhile to note, that the slope of the invariant mass spectrum is not affected by the expansion of the fireball, as it is the case for the momentum distributions of hadrons. Therefore, the measurement of the slope of the dilepton invariant mass spectrum at masses between 1 and 2 GeV/c^2 in heavy-ion collisions as a function of beam energy will allow the search for the caloric curve of QCD matter, and the discovery of both the onset of deconfinement and the critical endpoint of a possible 1st order phase transition.

Such an excitation function of the average fireball temperature T_{slope}, extracted from the dilepton invariant mass spectrum, is shown in Figure 8 as a red dashed line [40]. Up to a collision energy of $\sqrt{s_{NN}}$ = 6 GeV, the simulation was performed by applying a coarse-graining method to a hadronic UrQMD transport model calculation [41], whereas the high-energy part of T_{slope} as well as $T_{initial}$ was calculated with a fireball model [42]. The black square marks the data point from HADES [43], and the black triangle was extracted from NA60 data [44]. In addition, the freeze-out line is shown [32]. The upper limit for the temperature of a possible critical endpoint from a lattice QCD calculation is indicated as a green hatched area [26]. Consequently, Figure 8 represents an exclusion plot for the possible location of the critical endpoint of QCD matter in the plane temperature versus beam energy: The temperature of the critical endpoint is below the green area, and the beam energy is below $\sqrt{s_{NN}}$ = 6 GeV, where the freeze-out curve crosses the green area. Most probably, however, the upper limit of the beam energy is not much higher than the average temperature of the fireball T_{slope}, i.e., by the magenta line: This would result in a collision energy around $\sqrt{s_{NN}}$ = 3 GeV, corresponding to a net-baryon density of about 3.5 ρ_0, which is in the range of FAIR and NICA beam energies. Therefore, future dilepton experiments at these facilities have a unique discovery potential, and will either find a caloric curve or rule out the existence of a 1st order phase transition in dense QCD matter.

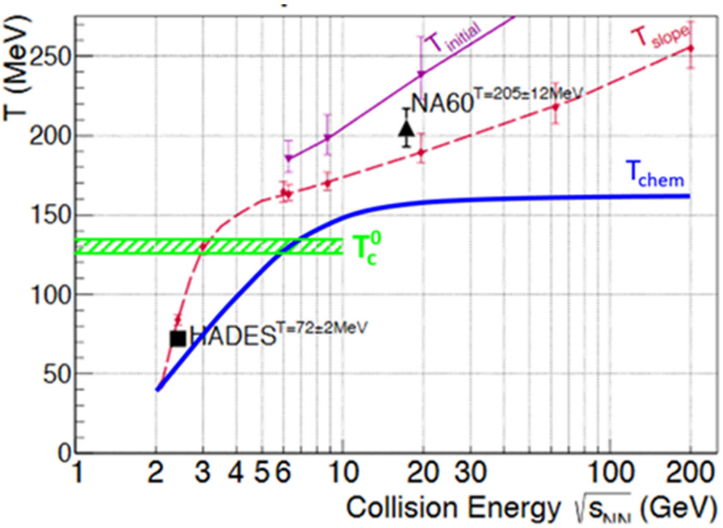

Figure 8. Fireball temperature as a function of heavy-ion collision energy [40]. The initial temperature $T_{initial}$ (purple line) and the average temperature T_{slope} (magenta dashed line) above $\sqrt{s_{NN}}$ = 6 GeV are calculated with a fireball model [42], whereas the low energy part of T_{slope} was simulated by a coarse-graining method applied to a transport model [41]. The black data points are from HADES [43] and NA60 [44]. The blue line represents the chemical freeze-out temperatures [32], and the green area marks the maximum temperature of the critical endpoint from lattice QCD [26].

5. Future Accelerator Centers FAIR and NICA

5.1. The Facility for Antiproton and Ion Research

The "Facility for Antiproton and Ion Research" (FAIR) is under construction in Darmstadt, Germany, and will cover a broad physics program based on intense beams of ions and antiprotons [45,46]. The working horse is the superconducting synchrotron SIS100 with a magnetic rigidity of 100 Tm, which will provide high-intensity primary and secondary beams. Rare, unstable isotopes with neutron or proton excess will be produced and analyzed by the Superconducting Fragment Separator, and guided to a variety of instruments operated by the NUSTAR collaboration. A major aim of the experiments is to measure the lifetime and mass of yet unknown unstable isotopes, which are expected to take part in the nucleosynthesis of heavy nuclei in supernova explosions and neutron star mergers, and, finally, to explore the origin of heavy elements. High-energy antiproton beams will be used by the PANDA experiment, which is located in the High-Energy Storage Ring, to conduct a research program on hadron physics. The APPA collaboration will perform a broad spectrum of experiments on atomic physics, plasma physics, radiation biology, and material science. Last but not least, the research program on high-density QCD matter will be executed by the Compressed Baryonic Matter (CBM) experiment, which will be discussed below in more detail. The layout of FAIR is shown in Figure 9. The existing GSI facility is sketched in blue, comprising the linear accelerator UNILAC, the synchrotron SIS18, the storage rings, and the experiments. The red lines represent the future facility, including the synchrotron SIS100, the high-energy beam lines to the CBM, NUSTAR, and APPA experiments, the production targets for secondary beams, the Super Fragment Separator (SFRS), and the Collector Ring (CR) and the High-Energy Storage Ring with the PANDA experiment.

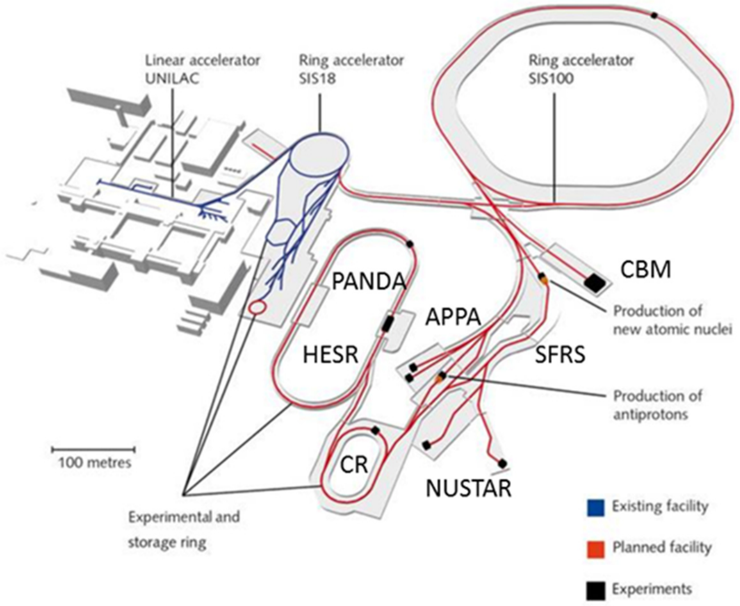

Figure 9. Layout of GSI and FAIR (see text) [45,46].

The investigation of high-density QCD matter, including the EOS and the phase diagram, will be performed with the CBM experiment at FAIR [47]. The envisaged high measurements of rare diagnostic probes will be performed with unprecedented reaction rates of up to 10 MHz, which require fast detectors, a free-streaming readout and acquisition system, and online event reconstruction and selection on a high-performance computing center. The vertex, track, and momentum measurement will be performed by the Micro-Vertex Detector (MVD) and a Silicon Tracking System (STS), both located in the gap of a large aperture superconducting dipole magnet. The MVD comprises four stations of Monolithic Active Pixel Sensors (MAPS), and the STS consists of eight stations with 900 double-sided micro-strip sensors. Downstream the magnet, a Ring Imaging Cherenkov (RICH) detector for electron identification is installed, which can be replaced by a Muon Chamber (MuCh) System, which consists of up to five hadron absorbers with triplets of tracking chambers in between. Behind these detector systems, a Transition Radiation

Detector (TRD) is installed, which either improves the identification of high-energetic electrons or is used as a final tracking station for the muons. A Time-of-Flight (TOF) wall with an active area of 120 m^2 behind the TRD consists of Multi-Gap Resistive Plate Chambers (MRPC). The polar angle acceptance of the total setup ranges from about 3 to 25°, in order to cover midrapidity. The reaction plane determination required for the measurement of the collective flow will be performed by a hadronic calorimeter, the Projectile Spectator Detector (PSD), positioned behind the TOF wall. The CBM experimental setup, which is sketched in the right part of Figure 10, shares the cave with the High-Acceptance Di-Electron Spectrometer (HADES, left part). HADES is already operational at SIS18, and is perfectly suited for reference measurements of hadrons and electrons with beams of protons and midsize nuclei due to its large polar angle acceptance from 18 to 85°.

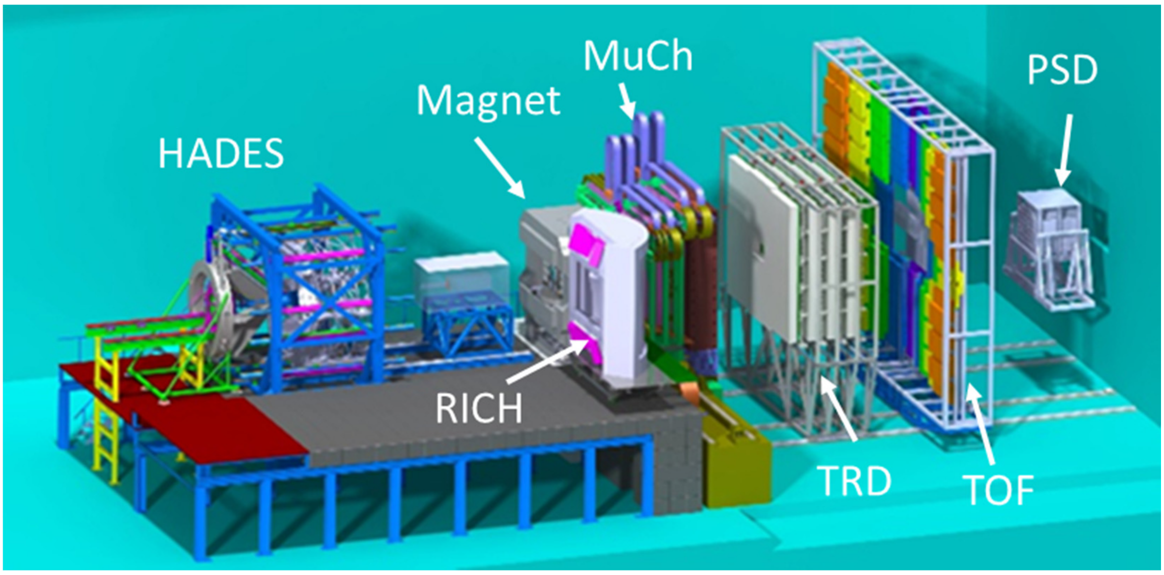

Figure 10. The CBM setup (**right**) and the HADES detector (**left**), which will be operated alternatively, with the beam coming from the left. The CBM muon detection system (MuCh) is in a measuring position, while the electron detector (RICH) is in a parking position. The HADES beam dump in front of the CBM magnet will be removed for the CBM operation.

5.2. The NICA Complex

The "Nuclotron-based Ion Collider fAcility" (NICA) is under construction at the Joint Institute for Nuclear Research (JINR) in Dubna, Russia [48]. The future heavy-ion beams at NICA will be accumulated and accelerated by the new superconducting Booster synchrotron, then stripped and injected into the Nuclotron synchrotron, which further accelerates the beams up to a magnetic rigidity of 45 Tm. The beams, for example, Au ions of 3.8A GeV kinetic energy with intensities of up to about 10^9 ions/s, can either be sent into the target hall or to the NICA collider, which reaches luminosities of 10^{27} cm^{-2} s^{-1} and collision energies of up to $\sqrt{s_{NN}}$ = 11 GeV. Figure 11 illustrates the layout of NICA. The Nuclotron hall hosts several setups, including the Baryonic Matter at Nuclotron (BM@N) experiment. Two experiments are located in the collider: The Multiple Purpose Detector (MPD), where the program on dense QCD matter will be performed, and the Spin Physics Detector (SPD), which uses polarized beams of protons and deuterons.

The Baryonic Matter at the Nuclotron (BM@N) experiment is already operational in two configurations since 2018. One version is used for experiments with beams of light and midsize ions and moderate intensities. It consists of a large acceptance dipole magnet with a gap size of 107 cm, where six triple Gas Electron Multiplier (GEM) tracking stations for track measurements of charged particles are located. In front of the GEMS, three planes of two-coordinate silicon detectors with a pitch of 95/103 µm are positioned. Downstream the magnet, two large Drift Chambers (DCH) for further tracking are installed, followed by two planes of TOF detectors, consisting of multi-Resistive Plate Chambers (mRPCs).

Behind the last TOF wall, a Zero-Degree Calorimeter is located in order to determine the reaction plane by measuring the spectator fragments. With this setup, lambda hyperons have been measured in collisions of a C beam with C, Al, and Cu targets at a kinetic energy of 4A GeV.

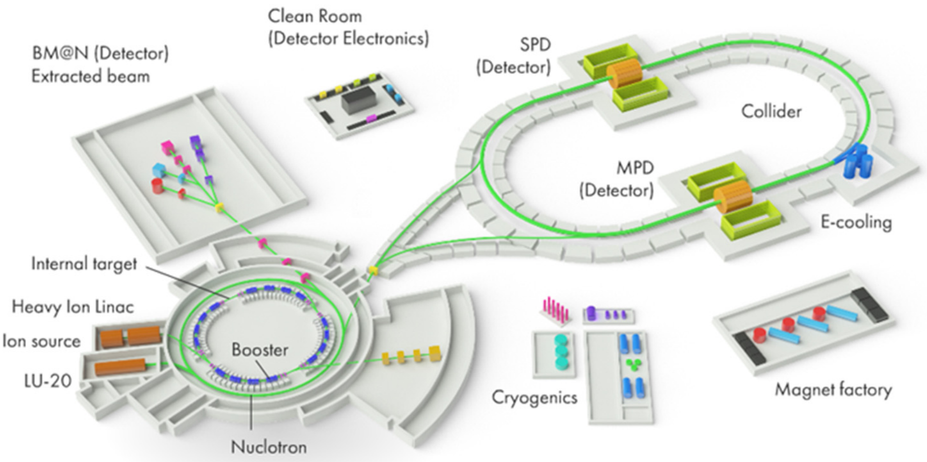

Figure 11. Layout of the NICA facility at JINR in Dubna (see text) [48].

The second BM@N detector configuration was used to study Short-Range Correlations (SRC). For this measurement, the setup was supplemented by a liquid hydrogen target and two additional detectors arms, each comprising a GEM and a TOF module for detecting the knock-out protons. With this setup, the first fully exclusive measurement in inverse kinematics probing the residual A-2 nuclear system was performed, where all the products of the reaction and ^{12}C + p $\rightarrow$ 2p + $^{10}{}_{4}$Be + p were identified [49].

In order to investigate the dense matter in Au + Au collisions at beam energies up to 3.8A GeV, the BM@N experiment has to be upgraded by four highly granular stations consisting of double-sided micro-strip silicon sensors. This detector system is presently jointly developed together with the CBM collaboration, which uses the same technology for the CBM experiment at FAIR. Moreover, a new Forward Hadron Calorimeter (FHCal) will be installed, which also uses modules developed for the CBM experiment. This setup will be well suited to measure observables sensitive to the equation-of-state of dense matter, such as the collective flow of identified particles, and the yield of multi-strange hyperons. A sketch of the upgraded BM@N experiment is shown in Figure 12 [50].

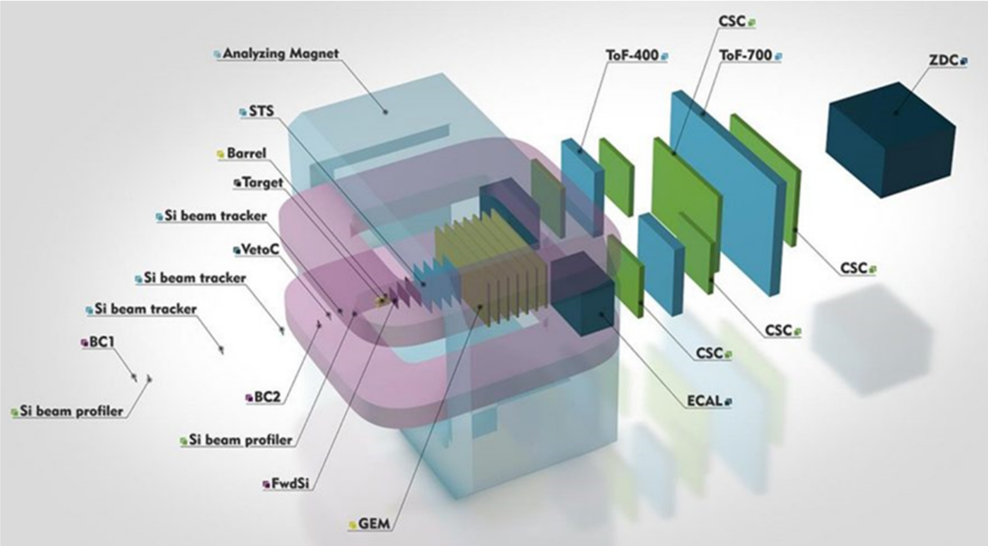

Figure 12. Sketch of the upgraded Baryonic Matter at the Nuclotron (BM@N) experiment [47].

The main experiment at NICA devoted to the study of the QCD phase diagram is the Multi-Purpose-Detector (MPD) at the collider [51]. The detector is designed to identify charged hadrons, electrons, and photons in heavy-ion collisions over a large solid angle close to 4π in Au + Au collisions at energies up to $\sqrt{s_{NN}}$ = 11 GeV and luminosities up to 10^{27} cm^{-2}s^{-1}, corresponding to a reaction rate of 6 kHz. The central detector is a Time-Projection Chamber (TPC), surrounded by a Time-of-Flight (TOF) barrel and an Electromagnetic Calorimeter (ECAL). These detectors are located inside a superconducting solenoid with a length of 5 m and a diameter of 4 m. Close to the beam pipe an Inner Tracking System (ITS) will be installed to measure the decay vertices of short-lived particles such as charmed mesons. The two forward spectrometers consist of Zero Degree Calorimeters (ZDC), Fast Forward Detectors (FFD), and Straw Tube Trackers (ECT). The technical challenge is to build the barrel detectors with a low material budget, as the average transverse momentum of the particles produced at NICA energies is below 500 MeV/c. The layout of the MPD setup is displayed in Figure 13 [48].

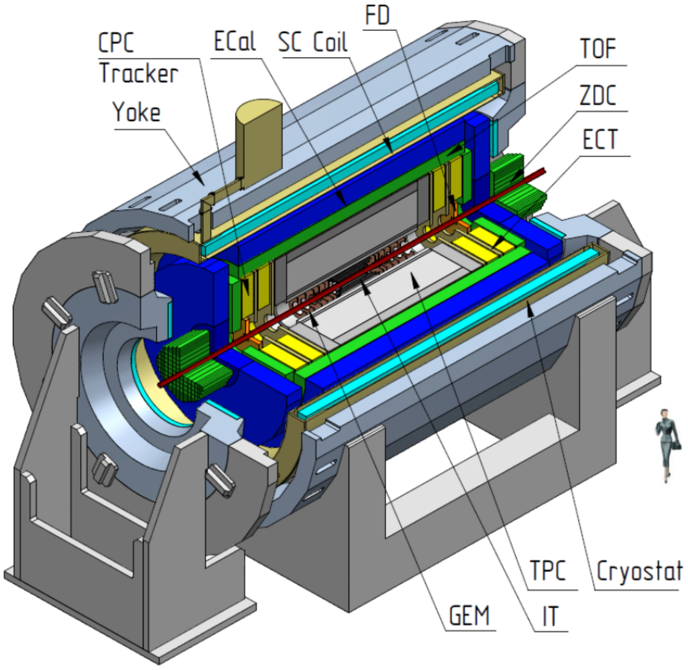

Figure 13. Layout of the MPD experiment at NICA (see text) [48].

5.3. Complementarity of the Experiments at FAIR and NICA

As outlined above, the common goal of the CBM experiment at FAIR, and the BM@N and MPD experiments at NICA is to investigate the properties of QCD matter at high baryon density. The successful execution of this research program requires the measurement of multi-dimensional and partly rare observables over a beam energy range, where high densities are created in heavy-ion collisions. Therefore, the rate capability of the experiments and the available beam energies are important prerequisites for discoveries. These two important features are plotted in Figure 14 for experiments under construction such as CBM, BM@N, and MPD, and for running experiments such as STAR at BNL-RHIC, NA61/SHINE at CERN-SPS, and HADES at GSI-SIS18. The plot demonstrates, that the luminosity at the colliders decreases drastically with the decreasing collision energy, whereas the reaction rates for fixed target experiments stay constant, as they are only limited by the rate capability of the detectors. For this reason, a fixed target was implemented in the STAR experiment, which allows measurements also in the CBM-FAIR energy range, although at much lower reaction rates. The lower energies are covered by HADES and BM@N, where Au beams up to kinetic energies of 1.23 and 3.8A GeV, respectively, are available. It is worthwhile to note, that HADES measures both hadrons and electrons, whereas BM@N is a hadron experiment. The CBM experiment, which has been optimized to run at extremely high rates up to 10 MHz, will run with Au beams at energies from 2 to 11A GeV, measuring hadrons, electrons, and muons. Higher energies are covered by the MPD at NICA. In conclusion, the future experiments at FAIR and NICA complement each other with respect to the collision energy and reaction rate.

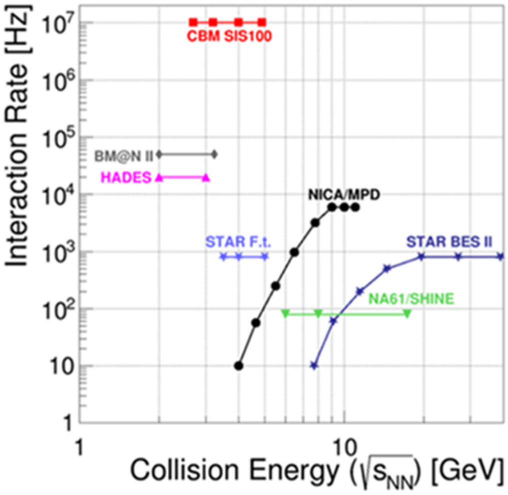

Figure 14. The Au + Au interaction rates as a function of collision energy for existing and emerging experiments (see text, taken from [47]). STAR F.t. stands for STAR fixed target mode.

6. Summary and Conclusions

The future experiments CBM at FAIR, BM@N, and MPD at NICA will open unique possibilities for the investigation of strongly-interacting matter at high baryon densities, including the determination of the EOS, and the study of elementary degrees-of-freedom. Up to now, the EOS has been constrained in laboratory experiments around saturation density ρ_0 with stable nuclei, and up to 2 ρ_0 using heavy-ion beams. For higher baryon densities, which are relevant for our understanding of neutron stars, only pioneering heavy-ion experiments have been performed at BNL, and the constraints on the EOS are much weaker. The CBM, BM@N, and the MPD experiments are designed to conduct precision measurements of collective flow of identified particles, multi-strange hyperons, and hypernuclei, in order to determine the high-density EOS, and to shed light on the hyperon puzzle in neutron stars. Another focus of these experiments is the exploration of the phase structure of dense QCD matter, including the search for a 1st order phase transition and its critical endpoint, which is predicted by lattice QCD calculations to be located in the beam energy range of FAIR and NICA, if it exists at all. Here, the relevant observables include excitation functions of higher-order fluctuations of the proton number distributions, multi-strange (anti-) hyperon production, and the fireball temperature extracted from the invariant-mass distributions of lepton pairs. In particular, the dilepton measurements which will be performed by CBM and MPD have a substantial discovery potential, as they will allow determining the caloric curve of dense QCD matter, and, hence, confirming or ruling out the existence of a 1st order phase transition.

In conclusion, the proposed laboratory measurements will complement astronomical observations devoted to the measurement of the mass and radius of neutron stars, and of gravitational waves from neutron star mergers, in order to constrain the EOS, and to elucidate the elementary structure of matter at neutron star core densities.

Funding: This research received no external funding.

Data Availability Statement: Not applicable.

Acknowledgments: The author acknowledges support from the Europeans Union's Horizon 2020 research and innovation programme under grant agreement no. 871072, and from RFBR according to the research project no. 18-02-40086 by the Ministry of Science and Higher Education of the Russian Federation, Project "Fundamental properties of elementary particles and cosmology" no. 0723-2020-0041.

Conflicts of Interest: The author declares no conflict of interest.

References

1. Klaehn, T.; Blaschke, D.; Typel, S.; van Dalen, E.; Faessler, A.; Fuchs, C.; Gaitanos, T.; Grigorian, H.; Ho, A.; Kolomeitsev, E.; et al. Constraints on the high-density nuclear equation of state from the phenomenology of compact stars and heavy-ion collisions. *Phys. Rev. C* **2006**, *74*, 035802. [CrossRef]
2. Fonseca, E.; Cromartie, H.T.; Pennucci, T.T.; Ray, P.S.; Kirichenko, A.Y.; Ransom, M.; Demorest, P.D.; Stairs, H. Refined Mass and Geometric Measurements of the High-Mass PSR J0740+6620. *arXiv* **2021**, arXiv:2104.00880.
3. Arzoumanian, Z.; Baker, P.T.; Brazier, A.; Burke-Spolaor, S.; Chamberlin, S.J.; Chatterjee, S.; Christy, B.; Cordes, J.M.; Cornish, N.J.; Crawford, F.; et al. The NANOGrav 11 Year Data Set: Pulsar-timing Constraints on the Stochastic Gravitational-wave Background. *Astrophys. J.* **2018**, *859*, 47. [CrossRef]
4. Available online: https://heasarc.gsfc.nasa.gov/docs/nicer/ (accessed on 15 May 2021).
5. Fukushima, K.; Kojo, T.; Weise, W. Hard-core deconfinement and soft-surface delocalization from nuclear to quark matter. *Phys. Rev. D* **2020**, *102*, 096017. [CrossRef]
6. Stone, J.R.; Stone, N.J.; Moszkowski, S.A. Incompressibility in finite nuclei and nuclear matter. *Phys. Rev. C* **2014**, *89*, 044316. [CrossRef]
7. Fuchs, C. The Nuclear Equation of State at high densities. *arXiv* **2006**, arXiv:nucl-th/0610038.
8. Le Fèvre, A.; Leifels, Y.; Reisdorf, W.; Aichelin, J.; Hartnack, C. Constraining the nuclear matter equation of state around twice saturation density. *Nucl. Phys. A* **2016**, *945*, 112–133. [CrossRef]
9. Wang, Y.; Guob, C.; Lia, Q.; Le Fevre, A.; Leifels, Y.; Trautmann, W. Determination of the nuclear incompressibility from the rapidity-dependent elliptic flow in heavy-ion collisions at beam energies 0.4A–1.0A GeV. *Phys. Lett. B* **2018**, *778*, 207–212. [CrossRef]
10. Sturm, C.; Böttcher, I.; Dębowski, M.; Förster, A.; Grosse, E.; Koczoń, P.; Kohlmeyer, B.; Laue, F.; Mang, M.; Naumann, L.; et al. Evidence for a soft nuclear equation of state from kaon production in heavy ion collisions. *Phys. Rev. Lett.* **2001**, *86*, 39. [CrossRef]
11. Fuchs, C.; Faessler, A.; Zabrodin, E.; Zheng, Y.-M. Probing the Nuclear Equation of State by K+ Production in Heavy-Ion Collisions. *Phys. Rev. Lett.* **2001**, *86*, 1974. [CrossRef] [PubMed]
12. Hartnack, C.; Aichelin, J. Analysis of kaon production around the threshold. *J. Phys. G* **2002**, *28*, 1649. [CrossRef]
13. Russotto, P.; Gannon, S.; Kupny, S.; Lasko, P.; Acosta, L.; Adamczyk, M.; Al-Ajlan, A.; Al-Garawi, M.; Al-Homaidhi, S.; Amorini, F. Results of the ASY-EOS experiment at GSI: The symmetry energy at supra-saturation density. *Phys. Rev. C* **2016**, *94*, 034608. [CrossRef]
14. Cozma, M.D. The impact of energy conservation in transport models on the π-/π+ multiplicity ratio in heavy-ion collisions and the symmetry energy. *Phys. Lett. B* **2016**, *753*, 166–172. [CrossRef]
15. Estee, J.; Lynch, W.G.; Tsang, C.Y.; Barney, J.; Jhang, G.; Tsang, M.B.; Wang, R.; Kaneko, M. Probing the Symmetry Energy with the Spectral Pion Ratio. *Phys. Rev. Lett.* **2021**, *126*, 162701. [CrossRef] [PubMed]
16. Miller, M.C.; Lamb, F.K.; Dittmann, A.J.; Bogdanov, S.; Arzoumanian, Z.; Gendreau, K.C.; Guillot, S.; Harding, A.K.; Ho, W.C.G.; Lattimer, J.M.; et al. PSR J0030+0451 Mass and Radius from NICER Data and Implications for the Properties of Neutron Star Matter. *Astrophys. J.* **2019**, *887*, L24. [CrossRef]
17. Pinkenburg, C.; Ajitanand, N.N.; Alexander, J.M.; Anderson, M.; Best, D.; Brady, F.P.; Case, T.; Caskey, W.; Cebra, D.; Chance, J.L. Elliptic Flow: Transition from Out-of-Plane to In-Plane Emission in Au + Au Collisions. *Phys. Rev. Lett.* **1999**, *83*, 1295. [CrossRef]
18. Danielewicz, P.; Lacey, R.; Lynch, W.G. Determination of the Equation of State of Dense Matter. *Science* **2002**, *298*, 1592–1596. [CrossRef]
19. Aichelin, J.; Bratkovskaya, E.; Fevre, A.L.; Kireyeu, V.; Kolesnikov, V.; Leifels, Y.; Voronyuk, V. Parton-Hadron-Quantum-Molecular Dynamics (PHQMD)—A Novel Microscopic N-Body Transport Approach for Heavy-Ion Collisions, Dynamical Cluster Formation and Hypernuclei Production. *Phys. Rev. C* **2020**, *101*, 044905. [CrossRef]
20. Logoteta, D.; Vidana, L.; Bombaci, I. Impact of chiral hyperonic three-body forces on neutron stars. *Eur. Phys. J. A* **2019**, *55*, 207. [CrossRef]
21. Weise, W. Dense Baryonic Matter and Strangeness in Neutron Stars. In Proceedings of the 8th International Conference on Quarks and Nuclear Physics (QNP2018), Tsukuba, Japan, 13–17 November 2018; p. 011002.
22. Andronic, A.; Braun-Munzinger, P.; Stachel, J.; Stöcker, H. Production of light nuclei, hypernuclei and their antiparticles in relativistic nuclear collisions. *Phys. Lett. B* **2011**, *697*, 203–207. [CrossRef]
23. Andronic, A.; Braun-Munzinger, P.; Redlich, K.; Stachel, J. Decoding the phase structure of QCD via particle production at high energy. *Nature* **2018**, *561*, 321–330. [CrossRef]
24. Aoki, Y.; Endrődi, G.; Fodor, Z.; Katz, S.D.; Szabó, K.K. The order of the quantum chromodynamics transition predicted by the standard model of particle physics. *Nature* **2006**, *443*, 675–678. [CrossRef] [PubMed]

25. Bazavov, A.; Bhattacharya, T.; Cheng, M.; De Tar, C.; Ding, H.-T.; Gottlieb, S.; Gupta, R.; Hegde, P.; Heller, U.M.; Karsch, F.; et al. The chiral and deconfinement aspects of the QCD transition. *Phys. Rev. D* **2012**, *85*, 054503. [CrossRef]
26. Ding, H.T.; Hegde, P.; Kaczmarek, O.; Karsch, F.; Lahiri, A.; Li, S.T.; Mukherjee, S.; Ohno, H.; Petreczky, P.; Schmidt, C.; et al. Chiral Phase Transition Temperature in (2 + 1)-Flavor QCD. *Phys. Rev. Lett.* **2019**, *123*, 062002. [CrossRef]
27. Fukushima, K.; Hatsuda, T. The phase diagram of dense QCD. *Rep. Prog. Phys.* **2011**, *74*, 014001. [CrossRef]
28. Blacker, S.; Bastian, N.-U.F.; Bauswein, A.; Blaschke, D.B.; Fischer, T.; Oertel, M.; Soultanis, T.; Typel, S. Constraining the onset density of the hadron-quark phase transition with gravitational-wave observations. *Phys. Rev. D* **2020**, *102*, 123023. [CrossRef]
29. Stephanov, M.A.; Rajagopal, K.; Shuryak, E.V. Event-by-event fluctuations in heavy ion collisions and the QCD critical point. *Phys. Rev. D* **1999**, *60*, 114028. [CrossRef]
30. STAR Collaboration; Adam, J.; Adamczyk, J.; Adams, J.R.; Adkins, J.K.; Agakishiev, G.; Aggawal, M.M.; Ahammed, Z.; Alekseev, I.; Anderson, D.M.; et al. Net-proton number fluctuations and the Quantum Chromodynamics critical point. *arXiv* **2020**, arXiv:2001.02852v2.
31. Becattini, F. An introduction to the Statistical Hadronization Model. *arXiv* **2009**, arXiv:0901.3643.
32. Cleymans, J.; Oeschler, H.; Redlich, K.; Wheaton, S. Comparison of chemical freeze-out criteria in heavy-ion collisions. *Phys. Rev. C* **2006**, *73*, 034905. [CrossRef]
33. Braun-Munzinger, P.; Magestro, D.; Redlich, K.; Stachel, J. Hadron production in Au–Au collisions at RHIC. *Phys. Lett. B* **2001**, *518*, 41–46. [CrossRef]
34. Braun-Munzinger, P.; Stachel, J.; Wetterich, C. Chemical Freeze-out and the QCD Phase Transition Temperature. *Phys. Lett. B* **2004**, *596*, 61–69. [CrossRef]
35. Andronic, A.; Braun-Munzinger, P.; Stachel, J. Thermal hadron production in relativistic nuclear collisions. *Acta Phys. Polon. B* **2009**, *40*, 1005–1012.
36. Agakishiev, G.; Balanda, A.; Bannier, B.; Bassini, R.; Belber, D.; Belyaev, A.; Blanco, A.; Bohmer, M.; Boyard, J.L.; et al.; HADES Collaboration. Hyperon production in Ar + KCl collisions at 1.76A GeV. *Eur. Phys. J. A* **2001**, *47*, 21. [CrossRef]
37. Andronic, A.; Braun-Munzinger, P.; Redlich, K.; Stachel, J. Charmonium and open charm production in nuclear collisions at SPS/FAIR energies and the possible influence of a hot hadronic medium. *Phys. Lett. B* **2008**, *659*, 149–155. [CrossRef]
38. Linnyk, O.; Bratkovskaya, E.L.; Cassing, W.; Stöcker, H. Charmonium dynamics in heavy ion collisions. *Nucl. Phys. A* **2007**, *786*, 183. [CrossRef]
39. Steinheimer, J.; Botvina, A.; Bleicher, M. Sub-threshold charm production in nuclear collisions. *Phys. Rev. C* **2017**, *95*, 014911. [CrossRef]
40. Tripolt, R.-A. Electromagnetic and weak probes: Theory. *Nucl. Phys. A* **2021**, *1005*, 121755. [CrossRef]
41. Galatyuk, T.; Hohler, P.M.; Rapp, R.; Seck, F.; Stroth, J. Thermal Dileptons from Coarse-Grained Transport as Fireball Probes at SIS Energies. *Eur. Phys. J. A* **2016**, *52*, 131. [CrossRef]
42. Rapp, R.; van Hees, H. Thermal Dileptons as Fireball Thermometer and Chronometer. *Phys. Lett. B* **2016**, *753*, 586–590. [CrossRef]
43. HADES Collaboration; Adamczewski-Musch, J.; Arnold, O.; Behnke, C.; Belounnas, A.; Belyaev, A.; Berger-Chen, J.C.; Biernat, J.; Blanco, A.; Blume, C.; et al. Probing baryon-rich matter with virtual photons. *Nat. Phys.* **2019**, *15*, 1040–1045. [CrossRef]
44. Specht, H.J. Thermal Dileptons from Hot and Dense Strongly Interacting Matter. *AIP Conf. Proc.* **2010**, *1322*, 1–10. [CrossRef]
45. Available online: https://fair-center.de (accessed on 15 May 2021).
46. Durante, M.; Indelicato, P.J.; Jonson, B.; Koch, V.; Langanke, K.; Meissner, U.-G.; Nappi, E.; Nilsson, T.; Stöhlker, T.; Widmann, E.; et al. All the Fun of the FAIR: Fundamental physics at the Facility for Antiproton and Ion Research. *Phys. Scr.* **2018**, *94*, 033001. [CrossRef]
47. CBM Collaboration; Ablyazimov, T.; Abuhoza, A.; Adak, R.P.; Adamczyk, M.; Agarwal, K.; Aggarwal, M.M.; Ahammed, Z.; Ahmad, F.; Ahmad, N.; et al. Challenges in QCD matter physics—The Compressed Baryonic Matter experiment at FAIR. *Eur. Phys. J. A* **2017**, *53*, 60. [CrossRef]
48. Available online: https://nica.jinr.ru/ (accessed on 16 May 2021).
49. Patsyuk, M.; Collaboration, T.B.; Kahlbow, J.; Laskaris, G.; Duer, M.; Lenivenko, V.; Segarra, E.P.; Atovullaev, T.; Johansson, G.; Aumann, T.; et al. Unperturbed inverse kinematics nucleon knockout measurements with a carbon beam. *Nat. Phys.* **2021**. [CrossRef]
50. Senger, P.; Dementev, D.; Heuser, J.; Kapishin, M.; Lavrik, E.; Murin, Y.; Maksymchuk, A.; Schmidt, H.R.; Schmidt, C.; Senger, A.; et al. Upgrading the BM@N experiment at NICA for studies of dense nuclear matter. *Particles* **2019**, *2*, 481–490. [CrossRef]
51. Kisiel, A.; MPD Collaboration. The MPD Experiment and JINR: Construction status and physics performance. *Nucl. Phys. A* **2021**, *1005*, 122006. [CrossRef]